Journal of Solid State Chemistry 183 (2010) 1835–1840

Contents lists available at ScienceDirect

Journal of Solid State Chemistry

journal homepage: www.elsevier.com/locate/jssc

Synthesis of porous and nonporous ZnO nanobelt, multipod, and hierarchical nanostructure from Zn-HDS

Eue-Soon Jang [a,*], Jung-Hee Won [b], Young-Woon Kim [c], Zhen Cheng [a], Jin-Ho Choy [d,*]

[a] Molecular Imaging Program at Stanford (MIPS) and Bio-X Program, Department of Radiology, Stanford University, 1201 Welch Road, Stanford, CA 94305, USA
[b] Hygiene Application Team, LG Household and Health Care, Daejeon 305-343, Republic of Korea
[c] School of Materials Science and Engineering, Seoul National University, Seoul 151-744, Republic of Korea
[d] Center for Intelligent Nano-Bio Materials (CINBM), Division of Nanosciences and Department of Chemistry, Ewha Womans University, Seoul 120-750, Republic of Korea

ARTICLE INFO

Article history:
Received 19 February 2010
Received in revised form
17 May 2010
Accepted 24 May 2010
Available online 2 June 2010

Keywords:
Zn based hydroxide double salts
Soft-solution process
ZnO nanobelts
Multipod
Hierarchical nanostructures

ABSTRACT

Zn based hydroxide double salts (Zn-HDS) with an interlayer spacing of 20 Å was produced by dissolving dumbbell-like ZnO crystal. The resulting Zn-HDS with a ribbon-like shape has a suitable morphology to explore the remarkably mild procedure for synthesis of ZnO nanobelts. We found that the intercalated water molecules into the Zn-HDS could play a key role in the ZnO nanobelts porosity. The nonporous ZnO nanobelts were successfully synthesized from the Zn-HDS by soft-solution process at 95 °C through mild dehydration agent as Na_2CO_3. As-synthesized ZnO nanobelts were grown along not only the [0 1 −1 0], but also the [2 −1 −1 0]. On the other hand, the porous ZnO nanobelts were obtained from the Zn-HDS by calcinations at 200 and 400 °C. In addition, flower-like ZnO multipod and hierarchical nanostructures were produced from the Zn-HDS by using of strong dehydration agent (NaOH) through hydrothermal reaction at 150 and 230 °C.

Published by Elsevier Inc.

1. Introduction

Zinc oxide (ZnO) crystal with a direct wide band gap (ΔE_g=3.37 eV) and large excition binding energy (60 meV) is the most useful semiconductor in numerous application fields such as room-temperature UV-laser [1,2], light-emitting-diode (LED) [3,4], photocatalyst [5], gas sensor [6–8], solar cell [9,10], piezoelectric device [11–13], and so on. In particular, the optical and electrical properties of the ZnO crystal sensitively depend on the size, shape, and orientation [5,14]. Therefore, their control has been the key issue in the nanomaterials engineering field. For this reason, tremendous nanostructures including nanorod [15], nanobelt [16], nanoplate [5], nanoring [17], nanohelix [18], multipod [19,20], and hierarchical nanostructure [21,22] have been competitively developed by a number of methods such as thermal vapor transport-condensation method [15–18], metal organic chemical vapor deposition (MOCVD) [2], electrochemical reaction [23], hydrothermal reaction [5,19–22], etc. Among them, the ZnO nanobelts with a rectangular cross section have unique opto-electronic properties due to its unusual shape and structure [16]. It is well demonstrated by recent success in field-effect transistor [24], nanoresonator [11–13], and spintronics [25] applications of the ZnO nanobelts. Conventional method for synthesis of the ZnO nanobelts is vapor transport and condensation process based on vapor–liquid–solid (VLS) mechanism at high temperature above 1400 °C [16]. Such an extreme condition for vaporization of precursor could induce many oxygen defects on surface of the ZnO nanobelts [26]. These specific defects hinder progress to the applications of ZnO in optoelectronic and lasing devices [1]. In this respect, mild processing is strongly demanded for the synthesis of the ZnO nanobelts. Soft-solution process based on hydrothermal reaction at low temperature (~100 °C) is a green chemical procedure in terms of low energy consumption and simplicity [1]. However, there are only few reports on the synthesis of the ZnO nanobelts due to its unusual growth habit against typical growth rate, [0 0 0 1] > [0 1 −1 0] > [0 0 0 −1], of the ZnO crystal [1,5]. Therefore, mixed product with the nanowires (~60%) and nanobelts (~40%) was usually obtained from the hydrothermal reaction as well reported by Hu et al. [27].

Herein, we systematically developed a new procedure to synthesize porous and nonporous ZnO nanobelts from zinc based hydroxyl double salts (Zn-HDS) with a lamella structure. This Zn-HDS with an interlayer spacing of 20.0 Å was obtained by dissolving dumbbell-like ZnO crystal. Such large interlayer spacing of the Zn-HDS was induced by co-intercalation of acetate and carbonate anions, and its layered structure was profitable for the development of ZnO nanobelts. The Zn-HDS was completely changed to the porous and nonporous ZnO nanobelts by calcinations and dehydration agent as sodium bicarbonate

* Corresponding authors.
E-mail addresses: euesoon@stanford.edu (E.-S. Jang), jhchoy@ewha.ac.kr (J.-H. Choy).

0022-4596/$ - see front matter Published by Elsevier Inc.
doi:10.1016/j.jssc.2010.05.025

(Na_2CO_3). We expect that the present mild procedure could be an alternative approach to produce the ZnO nanobelts instead of the VLS method with high energy consumption process. In addition, flower-like multipod and hierarchical ZnO nanostructures were produced from the Zn-HDS by using sodium hydroxide (NaOH) as strong dehydration agent. To the best of our knowledge, it is the first report on the synthesis of the ZnO multipod and hierarchical nanostructures from the Zn-HDS.

2. Experimental procedure

2.1. Thermal processing

Zinc acetate dihydrate ($Zn(CH_3COO)_2 \cdot 2H_2O$, 99%) and hexamethylenetetramine (HMTA, $(CH_2)_6N_4$, 99.5%) were purchased from Sigma Aldrich. As a nutrient solution, 0.1 M zinc acetate dihydrate and 0.1 M HMTA aqueous solutions were prepared in Teflon lined autoclave, which was maintained at 95 °C for various reaction time from 6 to 60 h in conventional furnace. The resulting products were collected by centrifuging, and then washed with deionized water to remove any residual organic salts. The porous ZnO nanobelts were produced from the Zn-HDS, which was obtained from the above hydrothermal reaction of 60 h, by calcinations at 400 °C for 3 h. For the synthesis of the nonporous ZnO nanobelts, Teflon lined autoclave including the Zn-HDS (0.5 g) and 0.5 M Na_2CO_3 aqueous solution was heated at 95 °C for 24 h. In addition, a flower-like ZnO crystal was obtained from the Zn-HDS product of hydrothermal reaction for 60 h by using of 0.01 M NaOH as dehydration agent under hydrothermal reaction at 150 °C for 3 h. On the other hand, hierarchical structures (30%) and multipod ZnO crystal (70%) were achieved by increasing hydrothermal temperature up to 230 °C.

2.2. Instrumentation and measurements

Morphologies of the resulting products were observed by field emission scanning electron microscope (FE-SEM, HITACHI, S-4300) and high resolution transmission electron microscope (HR-TEM, JEOL, JEM-3000 F) with 300 kV accelerating voltage. Phase identification of all the products was characterized by the powder X-ray diffractometer (XRD, PHILIPS, PW3710 with Ni filtered Cu–K_α radiation, $\lambda_\alpha = 1.54187$ Å), Fourier transform Infrared spectrometer (FT-IR, Jasco 200), and thermal gravity/differential thermal analyzer (TG/DTA). The TG/DTA thermal analysis of the Zn-HDS product was carried out in an air environment at a heating rate of 10 °C/min.

3. Results and discussion

From hydrothermal reaction for 6 h of the nutrient solution, including 0.1 M zinc acetate and 0.1 M HMTA solution, we obtained dumbbell (DB)-like ZnO twin crystals as shown in Fig. 1(a). At the reaction time of 12 h, star-like Zn-HDS with 5 μm in length was produced by dissolving the DB ZnO crystals as shown in Fig. 1(b). After the reaction time of 24 h, Fig. 1(c) shows that dimension of the Zn-HDS increased up to 30 μm and shape of the DB ZnO crystals changed to hexagonal tube *via* gradual dissolution. At further increased reaction time of 60 h, the DB ZnO crystal was almost dissolved, and we found hexagonal nanoplates with numerous apertures (the inset of Fig. 1(d)). In addition, the Zn-HDS was continuously grown by dissolving the DB ZnO crystal as shown in Fig. 1(d).

Fig. 2 shows a further detailed FE-SEM and HR-TEM images for the Zn-HDS generated by dissolving the DB ZnO crystal. According

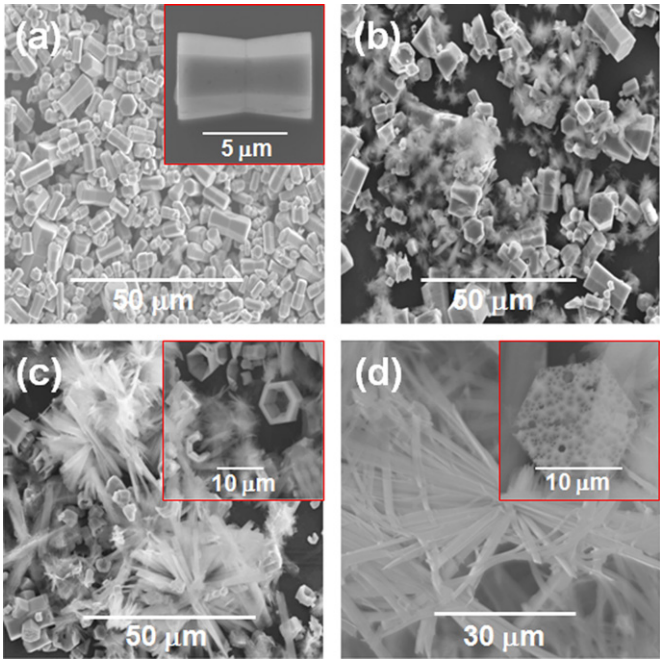

Fig. 1. Time resolved FE-SEM images of the resulting products obtained from soft-solution reaction times of (a) 6, (b) 12, (c) 24, and (d) 48 h.

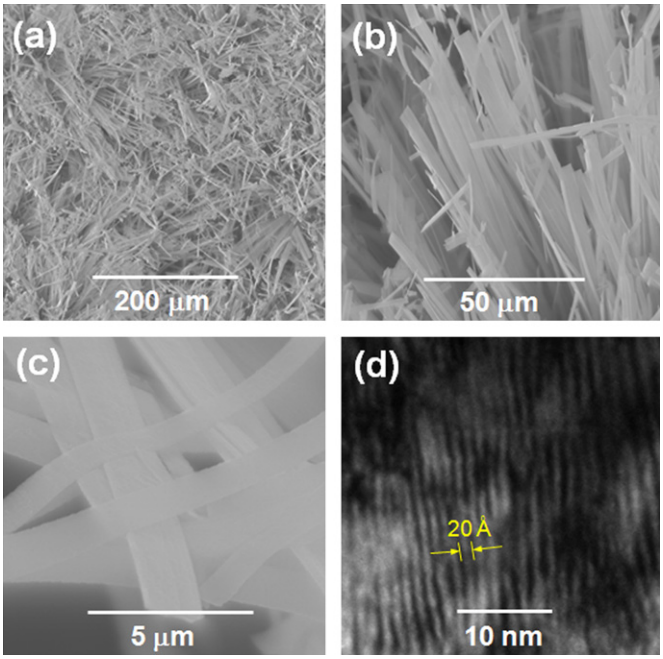

Fig. 2. (a–c) FE-SEM and (d) HR-TEM images of Zn-HDS with interlayer spacing of 20 Å.

to the low magnification FE-SEM image in Fig. 2 (a), the Zn-HDS was grown up to ~150 μm in length. As the high resolution images, Fig. 2(b) and (c) shows that the Zn-HDS has a ribbon-like shape with a width of 2 μm and thickness of 10 nm. Such well developed belt shape of the Zn-HDS is suitable to progress the ZnO nanobelt growth. HR-TEM image in Fig. 2(d) clearly shows layered structure of the Zn-HDS with an interlayer spacing of 20 Å.

In the electrostatic viewpoint, a positive charge of the Zn-HDS unit blocks ($[Zn_3^{oct}Zn_2^{tet}(OH)_8]^{2+}$) is the driving force for the

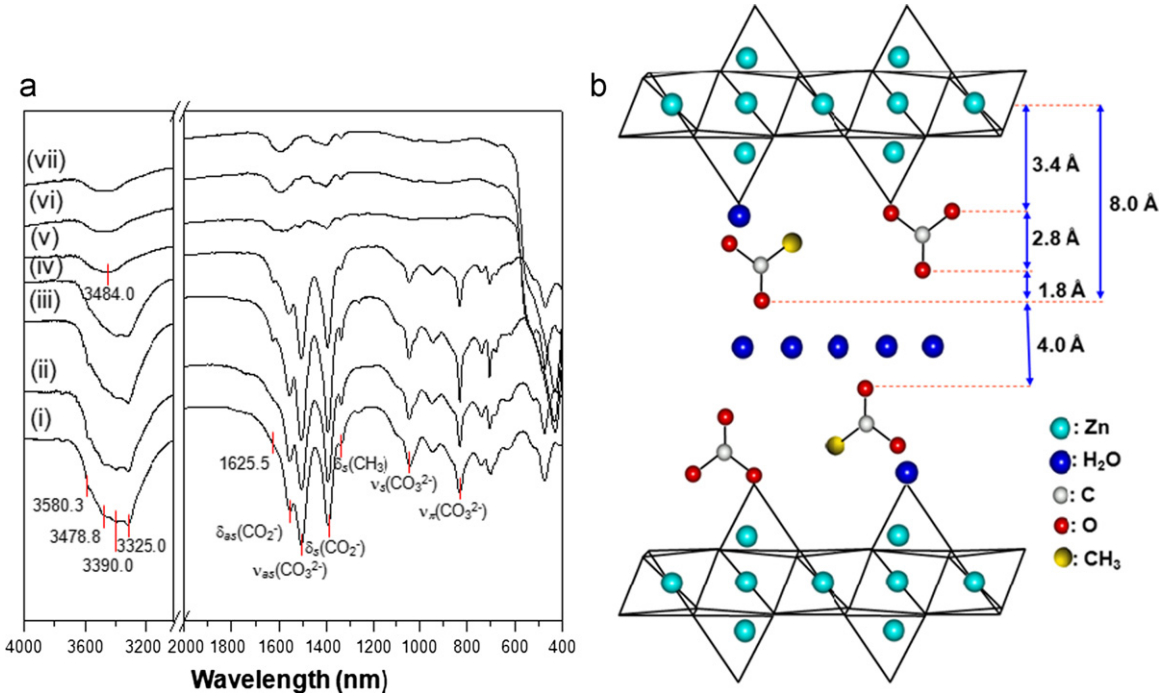

Fig. 3. (a) FT-IR spectra of Zn-HDS produced by heat treatment at (i) RT, (ii) 50, (iii) 100, (iv) 150, (v) 180, (vi) 200, and (vii) 250 °C; (b) schematic representation of Zn-HDS structure.

intercalation of various anion molecules [29]. In particular, positive Zn^{tet} ions occupied on tetrahedral sites play an important role in the intercalation reaction [29]. Identification of intercalated molecules could be characterized by FT-IR studies. As shown in Fig. 3(a)–(i), an FT-IR absorption feature of the Zn-HDS was corresponding to those of the typical carbonate and acetate anions [30,31]. In fact, we cannot obtain the carbonate intercalated Zn-HDS from the decarbonated water. This result implies that the intercalated CO_3^{2-} species come from the dissolved CO_2 into the nutrient solution. For the conjugation carbonate anion with Zn^{tet}, there are three different coordination structures as unidentate (C_s), bidentate (C_{2v}), and bridging coordination (C_{2v}). Among them, bridging coordination is forbidden due to the steady electric dipole moment (see Supporting Information) [31]. Therefore, the intercalated carbonate anion has unidentate or bidentate coordination state with the Zn^{tet} cation. As the symmetric C–O stretching mode ($\nu_s(CO_3^{2-})$), A_1' (ν_1) mode split into A_g+B_u and only B_u species is an IR active. In addition, doubly degenerated $E'(\nu_3)$ as the asymmetric C–O stretching mode ($\nu_{as}(CO_3^{2-})$) split into two bands as $A' + A''$ under the C_s and C_{2v} site symmetry (see Supporting Information) [31]. Fig. 3(a)-(i) clearly shows the $A_i(\nu_1)$ mode at 1043 cm^{-1} and the two $E'(\nu_3)$ modes at 1506.1 and 1392.4 cm^{-1}. It is indicating that the carbonate anions have C_s or C_{2v} site symmetry with the Zn^{tet} cations. According to the correlation between splitting value ($\Delta\nu_3$) of the ν_3 mode and coordination structure of the carbonate anion, the $\Delta\nu_3$ ($\sim$200 cm^{-1}) of the bidentate state is larger than that ($\sim$100 cm^{-1}) of the unidentate complex [31]. Therefore, the $\Delta\nu_3$ value of 113.7 cm^{-1} reveals that the carbonate anion in the present Zn-HDS has the unidentate coordination (C_s). On the other hand, we confirmed that the intercalated molecules are not only the carbonate, but also acetate anions, from which fingerprints of the methyl and carboxyl group were also observed as the symmetric bending mode ($\delta_s(CH_3)$) at 1338.4 cm^{-1} and an asymmetric stretch band ($\nu_{as}(CO_2^-)$) at 1552.4 cm^{-1} and symmetric one ($\nu_s(CO_2^-)$) at 1392.4 cm^{-1} as shown in Fig. 3(a)-(i) [30]. It indicates that the carbonate and acetate anions were co-intercalated into the Zn-HDS. According to Nakamoto, the separation values ($\Delta\nu_{as-s}$) between $\nu_{as}(CO_2^-)$ and $\nu_s(CO_2^-)$ bands are related to the coordination state of the acetate anion with a metal cation [31]. The present $\Delta\nu_{as-s}$ value of 160 cm^{-1} is indicating that the acetate anions are existing as a free ionic species and consequently the Zn^{tet} is completed by water molecules. Strong absorption peaks of the intercalated carbonate and acetate anions were observed even though increasing temperature up to 150 °C as shown in Fig. 3(a)-(ii)$\sim$(iv). Above 180 °C, the typical absorption peaks of the intercalated anions were significantly disappeared as shown in Fig. 3 (a)-(v)$\sim$(vii). It is indicating that transformation of the Zn-HDS to ZnO was induced above 180 °C. From the above FT-IR results, we suggest the crystal structure of the present Zn-HDS as shown in Fig. 3(b).

The general formula of HDS is $[(M^{2+}_{1-x}, M'^{2+}_{1+x})(OH)_{3(1-y)}]^{+}X^{n-}_{(1+3y)/n}\cdot zH_2O$, in which M and M' correspond to divalent transition metals (Cu, Co, Ni, Mn, and Zn) and X^{n-} is the intercalated anions [30]. In the present Zn-HDS, M and M' is Zn and X is CH_3COO^- and CO_3^{2-} as well explained by an FT-IR study. Therefore, formula of the present Zn-HDS could be represented as $[Zn_2(OH)_{3(1-y)}]^{+}[CH_3COO]_{(1+3y)}[CO_3]^{2-}_{(1+3y)/2}\cdot zH_2O$. From inductively coupled plasma (ICP) analysis, Zn concentration in 10 mg weight of the Zn-HDS was determined as 8.26×10^{-5} mol. In addition, Wt% of C, H, and N elements in 10 mg of the Zn-HDS was 4.9% (C), 3.0% (H), 0.0% (N). Therefore, the y and z parameters in the above formula of the Zn-HDS were determined as -0.198 and 1.2, respectively. Namely, composition stoichiometry of the present Zn-HDS is $Zn_2(OH)_{3.6}(CH_3CO_2^-)_{0.4}(CO_3^{2-})_{0.2}\cdot 1.2\ H_2O$.

The thermal gravity/differential thermal analyzer (TG/DTA) and temperature resolved XRD analysis for the Zn-HDS were systematically accomplished to find optimal calcinations temperature for the ZnO formation. The first weight loss occurred at 73.8 and 118.6 °C as endothermic peaks, as shown in Fig. 4(a). The former temperature corresponds to the departure of physically adsorbed water on the surface and the latter one implies the departure of intercalated water molecules into the Zn-HDS

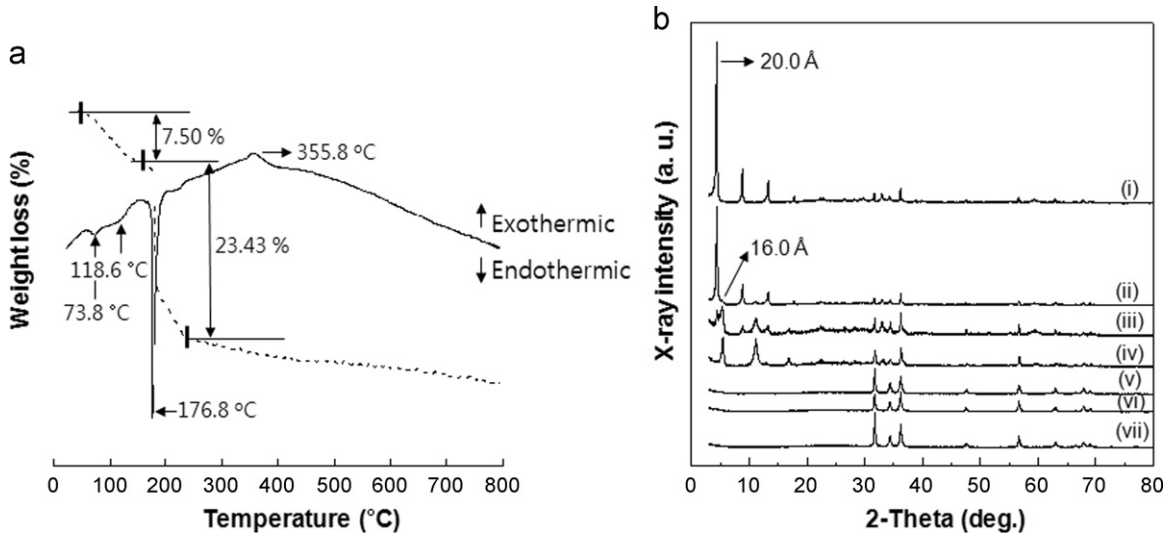

Fig. 4. (a) TG/DTA curves of Zn-HDS (heating rate is 5 °C/min); (b) XRD patterns of the resulting Zn-HDS obtained by heat treatment at (i) RT, (ii) 50, (iii) 100, (iv) 150, (v) 180, (vi) 200, and (vii) 250 °C.

[29,32]. The second weight loss with a strong endothermic peak at 176.8 °C is related to the transformation of the Zn-HDS to ZnO through the dehydroxylation of Zn hydroxide layer [29,32]. It is well consistent with the above FT-IR results. The third weight loss with an exothermic peak at 355.8 °C indicates the departure of CO_2 due to combustion of the intercalated carbonate and acetate molecules [29,32]. Temperature resolved XRD patterns were obtained by heating from room-temperature (RT) to 250 °C in the conventional furnace (Fig. 4(b)). For room temperature, the (0 0 l) peaks (l=1∼4) of the Zn-HDS were observed at 4.39, 8.80, 13.21, and 17.71 degree of 2θ (Fig. 4(b)-(i)). Basal spacing of the Zn-HDS was determined as 20 Å from the observed (0 0 l) peaks by using the Bragg equation, $n\lambda = 2d \sin\theta$, where n is an integer and λ is the wavelength (1.54056 Å) of an incident X-ray beam. As shown in Fig. 4(b)-(ii) and -(iii), the (0 0 l) peaks were shifted toward high angle, which the new (0 0 l) peaks are corresponding to the interlayer spacing of 16.0 Å, by heating at 50 and 100 °C. Fig. 4(b)-(iv) shows the interlayer distance of the Zn-HDS is completely changed from 20.0 to 16.0 Å by heating at 150 °C. This result implies disintercalation of the water molecules from interlayer of the Zn-HDS. Usually, eliminating temperature of the interlayer water is higher than the normal boiling temperature (100 °C) due to protection from the external thermal energy by the inorganic unit blocks [29]. One of the interesting facts is that such a decrease of the interlayer distance was immediately recovered from 16.0 to 20.0 Å under an ambient humidity condition for a few hours. It demonstrates that the water molecules play an important role in the electrostatic charge compensation between the intercalated molecules and building blocks. The decomposition of the Zn-HDS occurred at 180 °C and consequently the typical XRD patterns of the ZnO were observed, as shown in Fig. 4(b)-(v)∼(vii).

For the ZnO nanobelts formation, the Zn-HDS was heated at 400 °C for 3 h to completely eliminate the intercalated water and carbonate species. Fig. 5(b) shows the resulting products that the outer frame was still maintained, but the inner part was collapsed by creating many pores. Even though heat treatment at a lower temperature of 200 °C, we obtained only porous ZnO nanobelts as shown in Fig. 5(b). It clearly reveals that vaporization of the intercalated water molecules could influence on the Zn-HDS porosity. In order to synthesis the nonporous ZnO nanobelts, Na_2CO_3 was used as dehydration agent for elimination of the

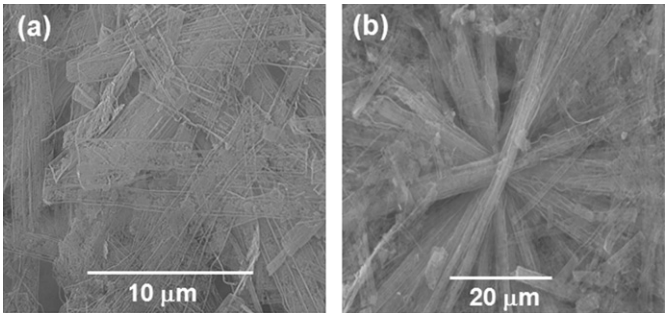

Fig. 5. FE-SEM images of porous ZnO nanobelts achieved from calcinations of Zn-HDS-60 h at (a) 400 °C and (b) 200 °C.

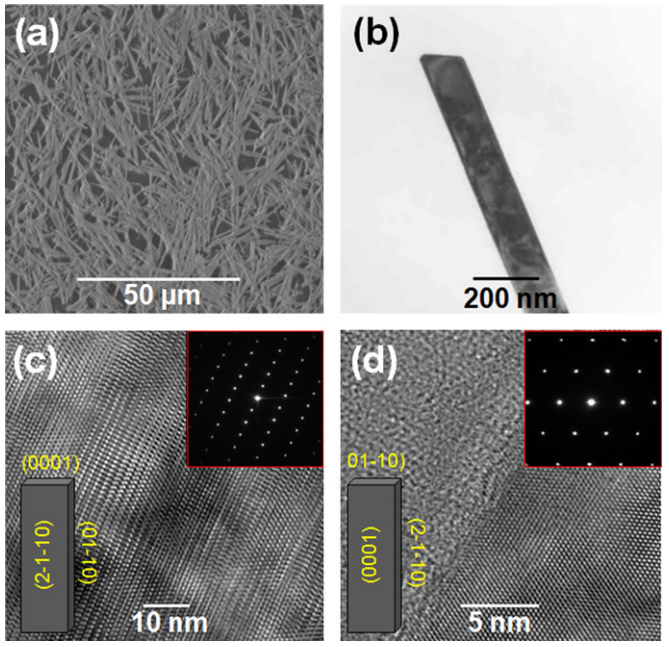

Fig. 6. (a) FE-SEM image and (b–d) TEM images and SAED patterns of nonporous ZnO nanobelt obtained from an anhydrous agent (Na_2CO_3) at 95 °C.

intercalated water molecules. After heat treatment at 95 °C for 24 h, Fig. 6(a) shows an FE-SEM image of the ZnO nanobelts without porosity. TEM image in Fig. 6(b) shows the typical ZnO nanobelt shape with rectangular edge. From the HR-TEM images and selected area electron diffraction (SAED) patterns in Fig. 6(c) and (d), we found that the present ZnO nanobelts have the dominated plane of the (2 −1 −1 0) or (0 0 0 1) surface as represented in the inset of Fig. 6(c) and (d) [33]. Namely, the as-synthesized ZnO nanobelts were grown along the [0 1 −1 0] or [2 −1 −1 0] direction. Such mixed growth direction could result from the nucleation seed growth with a different orientation. Fig. 7 shows XRD pattern of the ZnO nanobelts produced from the Zn-HDS by dehydration procedure *via* Na_2CO_3. There are no peaks corresponding to the Zn-HDS and any impurity components. In addition, intensity of the (*h k* 0) peaks is stronger than that of the (0 0 *l*) peaks. It is indicating that preferred growth orientation of the nanobelts is the [0 1 −1 0] direction.

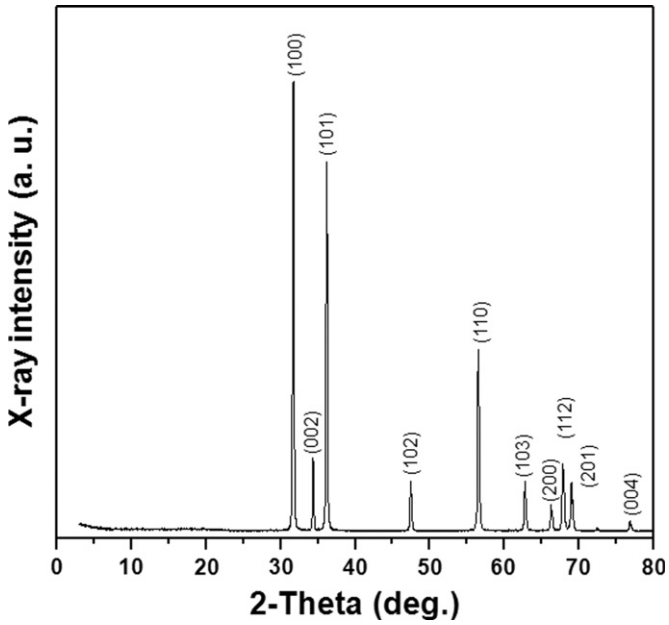

Fig. 7. XRD pattern of nonporous ZnO nanobelts.

On the other hand, a flower-like ZnO crystal was synthesized by using of 0.01 M NaOH as a strong dehydration agent under hydrothermal reaction at 150 °C for 3 h. Fig. 8(a) shows the flower-like ZnO crystals with ~50 μm in diameter. The high magnification FE-SEM images of Fig. 8(b) and (c) shows that the flower-like ZnO crystal consisted of many hexagonal rods with ~3 μm in length and ~1 μm in diameter. Growth mechanism of the ZnO multipod has been simply suggested by growing the nucleation seed, which was accidentally created into the nutrient solution [19,20]. However, growth mechanism of the nucleation seed for the ZnO multipod is still unclear. The present multipod ZnO crystal was produced from the Zn-HDS bundles with star-like shape. Therefore, destruction or dissolving rate of the center is much slower than that of the Zn-HDS edge. For this reason, the

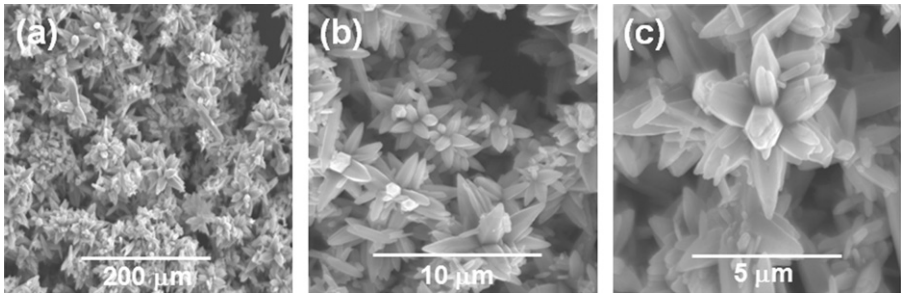

Fig. 8. FE-SEM images of flower-like ZnO multipod.

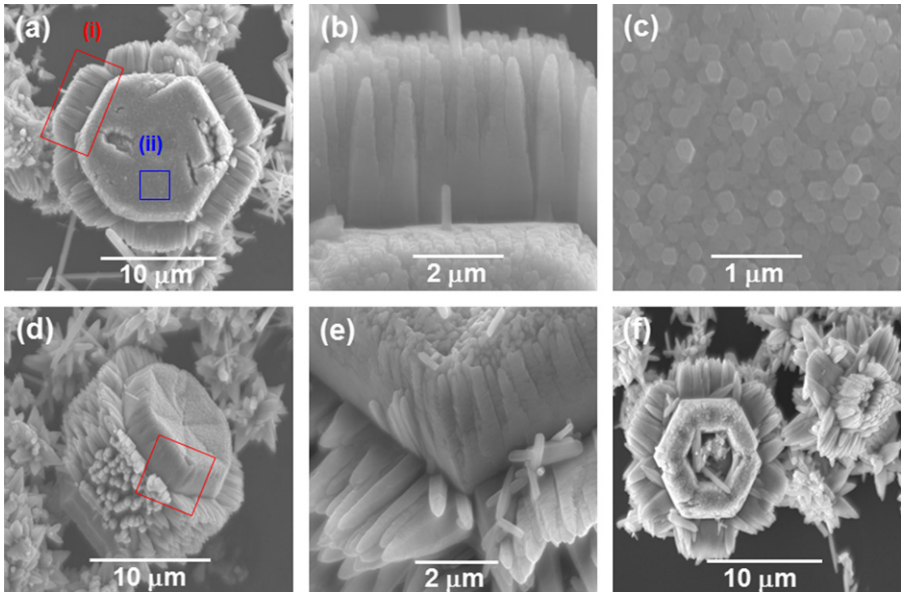

Fig. 9. FE-SEM images of hierarchical ZnO nanostructures.

nucleation seed with multi-domain for the ZnO multipod could be easily created during the dehydration reaction.

In addition, the hierarchical structures (30%) and the multipod crystal (70%) were achieved by hydrothermal reaction with NaOH solution at 230 °C. Fig. 9(a) shows a number of nanorods were grown on each side of a large hexagonal crystal. This hierarchical structure looks like a sunflower shape. From the high magnification image of square (i) denoted in Fig. 9(a), we found that the ZnO nanorods with 3 μm in length and 300 nm in diameter were densely grown on the side of hexagonal crystal as shown in Fig. 9(b). This hexagonal crystal with a diameter of 12 μm consisted of the hexagonal nanorods with a uniform diameter of 150 nm (Fig. 9(c)). Fig. 9(d) shows the side view of the hierarchical nanostructure with approximately 12 μm in length. The nanorods on the side were grown up over 7 μm thickness on the center. As the high magnification image of square denoted in Fig. 9(d), Fig. 9(e) shows that the nanorods were grown up to 4 μm in length. Some of the hierarchical nanostructure has a tube shape as shown in Fig. 9(f).

4. Conclusions

In conclusion, we systematically demonstrate the growth of the Zn-HDS from the DB ZnO crystal. During the dissolving progress, morphology of the DB ZnO crystal was changed to tube and nanoplates. As-synthesized Zn-HDS has a large interlayer spacing of 20 Å due to co-intercalation of acetate and carbonate anions. Ribbon-like shape of the Zn-HDS was suitable for the synthesis of the ZnO nanobelts. From the mild dehydration agent (Na_2CO_3), nonporous ZnO nanobelts with the preferred growth along the [0 1 −1 0] direction were successfully synthesized by soft-solution procedure. Porous ZnO nanobelts were also produced from the Zn-HDS by calcinations process. Moreover the flower-like ZnO multipod and hierarchical nanostructures were obtained from the Zn-HDS by using of the strong dehydration agent (NaOH) under hydrothermal reaction. The remarkably mild process for the ZnO nanobelts would be extremely advantageous not only in reducing the production cost, but also in accelerating the practical application of the ZnO nanobelts. In addition, the porous ZnO nanobelts, multipod, and hierarchical nanostructures with large surface area could be utilized for photocatalyst and gas sensor.

Acknowledgments

This work was supported by the Ministry of Education, Science and Technology (NRL project and BK 21 program), Korea Research Foundation (KRF, to E.-S. Jang) and Department of Radiology, Stanford University.

Appendix A. Supplementary materials

Supplementary data associated with this article can be found in the online version at doi:10.1016/j.jssc.2010.05.025.

References

[1] J. –H. Choy, E. –S. Jang, J. –H. Won, J. –H. Chung, D. –J. Jang, Y. –W. Kim, Adv. Mater. 15 (2003) 1911.
[2] E. –S. Jang, J.Y. Bae, J. Yoo, W.I. Park, D. –W. Kim, G. –C. Yi, T. Yatsui, M. Ohtsu, Appl. Phys. Lett. 88 (2006) 023102.
[3] A.M.C. Na, Y.Y. Xi, Y.F. Hsu, A.B. Djurišić, W.K. Chan, S. Gwo, H.L. Tam, K.W. Cheah, P.W.K. Fong, H.F. Lui, C Surya, Nanotechnology 20 (2009) 445201.
[4] A. Wadeasa, O. Nur, M. Willander, Nanotechnology 20 (2009) 065710.
[5] E. –S. Jang, J. –H. Won, S. –J. Hwang, J. –H. Choy, Adv. Mater. 18 (2006) 3309.
[6] J.X. Wang, X.W. Sun, Y. Yang, H. Huang, Y.C. Lee, O.K. Tan, L. Vayssieres, Nanotechnology 17 (2006) 4995.
[7] J.B.K. Law, J.T.L. Thong, Nanotechnology 19 (2008) 205502.
[8] J. Liu, Z. Guo, F. Meng, T. Luo, M. Li, J. Liu, Nanotechnology 20 (2009) 125501.
[9] Y. –J. Lee, D.S. Ruby, D.W. Peters, B.B. Mckenzie, J.W.P. Hsu, Nano Lett. 8 (2008) 1501.
[10] A.L. Briseno, T.W. Holcombe, A.I. Boukai, E.C. Garnett, S.W. Shelton, J.J.M. Fréchet, P. Yang, Nano Lett. 10 (2010) 334.
[11] Y. Qin, X. Wang, Z.L. Wang, Nature 451 (2008) 809.
[12] M. –P. Lu, J. Song, M. –Y. Lu, M. –T. Chen, Y. Gao, L. –J. Chen, Z.L. Wang, Nano Lett. 9 (2009) 1223.
[13] R. Yang, Y. Qin, C. Li, G. Zhu, Z.L. Wang, Nano Lett. 9 (2009) 1201.
[14] C. Kim, Y. –J. Kim, E. –S. Jang, G. –C. Yi, H.H. Kim, Appl. Phys. Lett. 88 (2006) 093104.
[15] M.H. Huang, S. Mao, H. Feick, H. Yan, Y. Wu, H. Kind, E. Weber, R. Russo, P. Yang, Science 292 (2001) 1897.
[16] Z.W. Pan, Z.R. Dai, Z.L. Wang, Science 291 (2001) 1947.
[17] X.Y. Kong, Y. Ding, R.S. Yang, Z.L. Wang, Science 303 (2004) 1348.
[18] P.X. Gao, Y. Ding, W.J. Mai, W.L. Hughes, C.S. Lao, Z.L. Wang, Science 309 (2005) 1700.
[19] M. Yang, G. Pang, L. Jiang, S. Feng, Nanotechnology 17 (2006) 206.
[20] R. Wahab, S.G. Ansari, Y.S. Kim, M. Song, H. –S. Shin, Appl. Surf. Sci. 255 (2009) 4891.
[21] T. Zhang, W. Dong, M.K. Brewer, S. Konar, R.N. Njabon, Z.R. Tian, J. Am. Chem. Soc. 128 (2006) 10960.
[22] T.L. Sounart, J. Liu, J.A. Voigt, M. Huo, E.D. Spoerke, B. McKenzie, J. Am. Chem. Soc. 129 (2007) 15786.
[23] J. Yang, Y. Qiu, S. Yang, Cryst. Growth Des. 7 (2007) 2562.
[24] Y.K. Park, A. Umar, E.W. Lee, D.M. Hong, Y. –B. Hahn, J. Nanosci. Nanotech. 9 (2009) 5745.
[25] C. Ronning, P.X. Gao, Y. Ding, Z.L. Wang, D. Schwen, Appl. Phys. Lett. 84 (2004) 783.
[26] L.S. Mende, J.L.M. Driscoll, Mater. today 10 (2007) 40.
[27] H. Hu, X. Huang, C. Deng, X. Chen, Y. Qian, Mater. Chem. Phys. 106 (2007) 58.
[29] H. Morioka, H. Tagaya, M. Karasu, J. Kadokawa, K. Chiba, Inorg. Chem. 38 (1999) 4211.
[30] L. Poul, N. Jouini, F. Fiévet, Chem. Mater. 12 (2000) 3123.
[31] K. Nakamoto, in: Infrared and Raman Spectra of Inorganic and Coordination Compounds, Part B: applications in Coordination, Organometallic, and Bioinorganic Chemistry, 5th ed., Wiley-Interscience, New York, 1997.
[32] E. Kandare, J.M. Hossenlopp, Inorg. Chem. 45 (2006) 3766.
[33] Z.L. Wang, Mater. Sci. Eng. 64 (2009) 33.